

THE DAMPING TAIL OF CMB ANISOTROPIES

Wayne Hu

Institute for Advanced Study, School of Natural Sciences,
Princeton, NJ 08540

and

Martin White

Enrico Fermi Institute, University of Chicago,
Chicago, IL 60637

ABSTRACT

By decomposing the damping tail of CMB anisotropies into a series of transfer functions representing individual physical effects, we provide ingredients that will aid in the reconstruction of the cosmological model from small-scale CMB anisotropy data. We accurately calibrate the model-independent effects of diffusion and reionization damping which provide potentially the most robust information on the background cosmology. Removing these effects, we uncover model-dependent processes such as the acoustic peak modulation and gravitational enhancement that can help distinguish between alternate models of structure formation and provide windows into the evolution of fluctuations at various stages in their growth.

Subject headings: cosmology:theory – cosmic microwave background.

Submitted: September 10, 1996 to ApJ

1. Introduction

Much effort is being expended to measure the angular power spectrum of the cosmic microwave background (CMB) anisotropy on increasingly smaller angular scales. For many types of models for structure formation, the spectrum can be predicted to a precision of about 1% (Hu et al. 1995), raising the hope that the cosmological parameters that are the input to these calculations can be extracted to comparable precision (see e.g. Jungman et al. 1996). The “inverse problem” of reconstructing the model given a spectrum is less well understood than the “forward problem” of predicting it given the model. For this purpose, it is important to assess the generation of anisotropies in a manner that is not tied to any given model for structure formation. From the theory of anisotropy formation, we know that CMB fluctuations suffered causal processing and damping of the primordial signal. In this paper, we numerically calibrate such effects, extending and improving upon prior work (Hu & Sugiyama 1995ab, 1996, hereafter HSc, HSb, HSc and Hu & White 1996b).

A particularly fruitful way to visualize the CMB spectrum, and one that provides a framework for the inverse problem, is as a product of transfer functions representing individual physical effects. The spectrum is then constructed out of physical elements rather than a model-dependent parameterization. Conceptually,

the evolution of CMB anisotropies processes primordial metric or gravitational potential perturbations into features observable in the spectrum today (see e.g. Bond 1996, Hu & White 1996b). Since the evolution obeys linear perturbation theory, its effects are described by a series of transfer functions that multiply the underlying perturbations. The form of these functions depends on the cosmological model, not only for the background expansion and thermal history (see e.g. Bond et al. 1994, Seljak 1994, Hu, Sugiyama & Silk 1996) but also for structure formation (see e.g. Crittenden & Turok 1995, Magueijo et al. 1996, Durrer et al. 1996, Hu, Spergel, & White 1996). By decomposing the evolution into functions representing separate physical effects, we can isolate portions of the anisotropy spectrum that are the most sensitive to particular aspects of the cosmological model.

In particular, processes that damp CMB anisotropies, photon diffusion (Silk 1968) and rescattering (Efstathiou & Bond 1987), depend mainly on the background parameters and little on the perturbations that form structure in the universe. In §2, we isolate these effects in a numerical treatment. From this damping calibration, we produce convenient fitting formulae that accurately describe the behavior of the diffusion and reionization damping transfer functions, or envelopes, directly in anisotropy multipole space. In §3, we illustrate the reconstruction process by testing it with known models within the cold dark matter (CDM) scenario. By removing the model-independent effects of damping, one uncovers important model-dependent effects such as the baryon-drag modulation of the peaks (HSa), the potential envelope that describes gravitational driving of acoustic oscillations (HSc), and the regeneration of anisotropies during reionization (Sunyaev & Zel’dovich 1970, Kaiser 1984).

In the context of currently popular models, recovery of these signatures will help distinguish between such possibilities as an inflationary or cosmological defect origin of fluctuations (Crittenden & Turok 1995, Durrer et al. 1996, Hu & White 1996b). The effects of damping are also intrinsically interesting because they provide the most model-independent probes of the background cosmology. We also consider how diffusion damping can be used to constrain the curvature of the universe and reionization damping to determine the redshift and extent of reionization in the universe. In this way, the study of effects in the damping tail of CMB anisotropies presented here will aid in the future reconstruction of the cosmological model from the anisotropy data.

2. Damping Calculation

Damping processes which affect CMB anisotropies provide the most model-independent information available in the spectrum and allow constraints on cosmological parameters such as the curvature and the thermal history of the universe. Furthermore, these universal effects obscure the model-*dependent* signatures that are useful to determine the mechanism for structure formation in the universe and the ultimate source of density perturbations.

For both these reasons, an accurate calibration of damping effects is desirable. In this section, we begin with the formalism necessary to describe them (§2.1) and simple approximations to help understand their nature (§2.2). We then turn to numerical calibration of these effects (§2.3). Finally, we give convenient fitting formulae to their effects on the anisotropy power spectrum that encapsulate these results (§2.4).

2.1. Boltzmann Formalism

In this section, we provide the formalism for the evolution of CMB anisotropies that underly the calculations which follow. It may be skimmed upon first reading.

The anisotropy in the CMB is described by small perturbations of the photon distribution function around a homogeneous and isotropic black-body. The Boltzmann equation describes the evolution of the distribution function f , through Compton scattering with electrons $df/d\eta(\eta, \mathbf{x}(\eta), \mathbf{p}(\eta)) = C[f]$, where the collision term is written schematically as $C[f]$. Here η is the conformal time and \mathbf{p} the photon momentum. In the absence of spectral distortions, the magnitude of the momentum can be integrated over leaving only its directional dependence γ and the effect of gravitational redshifts on the photon temperature perturbation Θ . Due to azimuthal symmetry and the decoupling of modes in linear theory, it is convenient to decompose the fluctuation in a Fourier or normal mode k into angular moments, e.g. in flat space $\Theta(\eta, \mathbf{k}, \gamma) = \sum_{\ell} (-i)^{\ell} \Theta_{\ell} P_{\ell}(\mathbf{k} \cdot \gamma)$ with an appropriate generalization to curved spaces (Wilson 1983, White & Scott 1996). Here γ_i are the direction cosines of the photon momenta. The Boltzmann equation then becomes an infinite hierarchy of coupled ordinary differential equations (see e.g. Ma & Bertschinger 1995)

$$\begin{aligned}\dot{\Theta}_0 &= -\frac{k}{3}\Theta_1 - \dot{\Phi}, \\ \dot{\Theta}_1 &= k \left[\Theta_0 + \Psi - \frac{2}{5}\kappa_2\Theta_2 \right] - \dot{\tau}(\Theta_1 - v_b), \\ \dot{\Theta}_2 &= k \left[\frac{2}{3}\kappa_2\Theta_1 - \frac{3}{7}\kappa_3\Theta_3 \right] - \dot{\tau} \left(\frac{9}{10}\Theta_2 - \frac{1}{10}Q_2 - \frac{1}{2}Q_0 \right), \\ \dot{\Theta}_{\ell} &= k \left[\frac{\ell}{2\ell-1}\kappa_{\ell}\Theta_{\ell-1} - \frac{\ell+1}{2\ell+3}\kappa_{\ell+1}\Theta_{\ell+1} \right] - \dot{\tau}\Theta_{\ell}, \quad (\ell > 2)\end{aligned}\tag{1}$$

where $\kappa_{\ell} = [1 - (\ell^2 - 1)K/k^2]^{1/2}$ modifies the angular hierarchy for geodesic deviation in spaces of constant comoving curvature $K = -H_0^2(1 - \Omega_0 - \Omega_{\Lambda})$ with a Hubble constant of $H_0 = 100h \text{ km s}^{-1} \text{ Mpc}^{-1}$. The metric perturbations are represented by Φ the fluctuation of the spatial curvature in Newtonian gauge and Ψ the Newtonian potential. The collision terms from $C[f]$ are proportional to $\dot{\tau} = n_e \sigma_T a$ the differential optical depth to Compton scattering, where n_e is the free electron density and σ_T is the Thomson cross section.

Scattering by electrons with velocity v_b generates a Doppler effect on the photons. Scattering of anisotropic radiation creates a polarization, described by the temperature perturbation in the Stokes parameter Q , and governed by a separate hierarchy (Bond & Efstathiou 1984),

$$\begin{aligned}\dot{Q}_0 &= -\frac{k}{3}Q_1 - \dot{\tau} \left[\frac{1}{2}Q_0 - \frac{1}{10}(\Theta_2 + Q_2) \right], \\ \dot{Q}_1 &= k \left[Q_0 - \frac{2}{5}\kappa_2Q_2 \right] - \dot{\tau}\Theta_1, \\ \dot{Q}_2 &= k \left[\frac{2}{3}\kappa_2Q_1 - \frac{3}{7}\kappa_3Q_3 \right] - \dot{\tau} \left(\frac{9}{10}Q_2 - \frac{1}{10}\Theta_2 - \frac{1}{2}Q_0 \right), \\ \dot{Q}_{\ell} &= k \left[\frac{\ell}{2\ell-1}\kappa_{\ell}Q_{\ell-1} - \frac{\ell+1}{2\ell+3}\kappa_{\ell+1}Q_{\ell+1} \right] - \dot{\tau}Q_{\ell}, \quad (\ell > 2).\end{aligned}\tag{2}$$

To complete these equations, we need the baryon Euler equation, which determines the evolution of the

baryon velocity,

$$\dot{v}_b = -\frac{\dot{a}}{a}v_b + k\Psi + \dot{\tau}(\Theta_1 - v_b)/R. \quad (3)$$

Finally, the observable anisotropy spectrum follows by integrating over the k -modes,

$$\frac{2\ell+1}{4\pi}C_\ell = \frac{1}{2\pi^2} \int \frac{dk}{k} \frac{k^3 |\Theta_\ell(\eta_0, k)|^2}{2\ell+1}. \quad (4)$$

The interpretation of these equations is quite straightforward. The metric fluctuations feed power into hierarchy through the gravitational redshift effects of density dilution ($\dot{\Phi}$ in $\ell = 0$) and potential infall ($k\Psi$ in $\ell = 1$). If the optical depth across a wavelength $\dot{\tau}/k \ll 1$, this power flows to higher ℓ much like a wave pulse flows along a string, being concentrated in mode ℓ when $k\eta \sim \ell$. The critical epoch for this process is horizon crossing $k\eta \sim 1$ after which $\ell \gtrsim 1$ modes can be populated. When the free electron density is not negligible then the Compton scattering terms ($\dot{\tau}$ terms) become important. Modes with $\ell \geq 2$ are exponentially damped, sealing off the hierarchy and providing a barrier off which the wave pulse reflects. The monopole term is not damped at all and the dipole term is driven toward v_b so that the distribution is isotropic in the electron rest frame.

Thus before recombination, $\dot{\tau}/k \gg 1$, and the photon distribution possesses only the $\ell = 0$ (density) and $\ell = 1$ (velocity) modes, which represent a fluid that oscillates acoustically due to photon pressure (see §2.2). Only for very high k will power leak into the higher ℓ modes, where it will be exponentially damped. This is responsible for the damping tail at small angular scales. An increase in $\dot{\tau}$ at late times due to reionization also possesses a characteristic signature. For scales inside the horizon at reionization, the power has already propagated to high ℓ where it suffers exponential damping; for larger scales no such damping occurs. Thus reionization damps small-scale anisotropies while preserving large-scale anisotropies. We shall discuss these behaviors more quantitatively in the next section.

2.2. Analytic Estimates

Before turning to the numerical calibration of effects in the damping tail, it is useful to describe them analytically to see how they enter in and affect the Boltzmann evolution given above. The two main damping processes at work in the CMB are photon diffusion before recombination and rescattering during an epoch of late reionization.

2.2.1. Diffusion Damping before Recombination

For wavelengths much larger than the mean free path to Compton scattering ($k/\dot{\tau} \ll 1$), the Boltzmann hierarchy of Eq. (1) can be described by the relativistic fluid dynamics of a combined photon-baryon fluid. Rapid scattering insures that any anisotropy of the photons in the electron rest frame is vanishingly small so that the hierarchy can be truncated at $\ell = 1$ with $\Theta_1 \approx v_b$. Even in this *tightly-coupled* regime, the random walk of the photons through the electrons eventually mixes photons across a wavelength of the fluctuation (Silk 1968). Thus, we expect temperature perturbations to be destroyed by this diffusive process *before* the mean free path grows long enough to invalidate the central approximation. This statement is only approximately true during the recombination epoch when the mean free path grows so rapidly that it approaches the horizon scale and coincides with the diffusion scale. For this reason, we calibrate the process numerically in §2.3.

Formally, we can approximate these effects by expanding the Boltzmann temperature and polarization equations (1) and (2) in powers of $k/\dot{\tau}$ (Peebles & Yu 1970). To lowest order, one obtains the oscillator equation (HSa)

$$\frac{d}{d\eta}(1+R)\dot{\Theta}_0 + \frac{k^2}{3}\Theta_0 = -\frac{k^2}{3}(1+R)\Psi - \frac{d}{d\eta}(1+R)\dot{\Phi}. \quad (5)$$

Gravity drives the oscillator by potential infall into Ψ and density dilution as the curvature fluctuation Φ changes. The baryon inertia in the fluid is described by the relative baryon-photon momentum density ratio R and increases the effective mass of the oscillator. Together these effects imply oscillations at the sound speed

$$c_s = \frac{1}{\sqrt{3(1+R)}}, \quad (6)$$

around a zero point displaced by gravity to $(1+R)\Psi$ for slowly-varying Φ (HSa, HSc, Hu & White 1996b).

To treat the effects of diffusion, one must include higher order terms. An examination of the $\ell = 1$ photon Euler equation (1) shows that there are two diffusive effects: viscous damping from the quadrupole Θ_2 and heat conduction from the relative photon-baryon velocity $\Theta_1 - v_b$ (Weinberg 1972). From the expansion of the polarization hierarchy, $Q_2 = Q_0 = \frac{1}{4}\Theta_2$ and the quadrupole evolution equation (1) with $\Theta_1 \gg \Theta_3$, we obtain the tight-coupling prediction for the quadrupole,

$$\Theta_2 = (k/\dot{\tau})\frac{8}{9}\Theta_1. \quad (7)$$

Heat conduction may be described by expanding the baryon Euler equation (3) to second order. Let us assume a solution of the form $\Theta_1 \propto \exp i \int \omega d\eta$ and ignore variations on the expansion time scale \dot{a}/a in comparison with those at the oscillation frequency ω . We return to consider this approximation in §3.1. The heat conduction equation becomes

$$\Theta_1 - v_b = \dot{\tau}^{-1}R[i\omega\Theta_1 - k\Psi] + \omega^2\dot{\tau}^{-2}R^2\Theta_1, \quad (8)$$

allowing us to rewrite the photon Euler equation (1) as

$$i\omega(1+R)\Theta_1 = k[\Theta_0 + (1+R)\Psi] - \omega^2\dot{\tau}^{-1}R^2\Theta_1 - \frac{16}{45}k^2\dot{\tau}^{-1}\Theta_1. \quad (9)$$

The presence of $(1+R)\Psi$ again reflects the gravitational zero-point displacement of the oscillator. It is thus appropriate to try a solution of the form $\Theta_0 + (1+R)\Psi \propto \exp i \int \omega d\eta$. With this assumption, one obtains the dispersion relation for acoustic oscillations

$$\omega = \pm kc_s + i\frac{1}{6}k^2\dot{\tau}^{-1} \left[\frac{R^2}{(1+R)^2} + \frac{16}{15} \frac{1}{1+R} \right]. \quad (10)$$

From the form of the solution $\exp i \int \omega d\eta$, this gives the damping scale k_D (Kaiser 1983)

$$k_D^{-2} = \frac{1}{6} \int d\eta \frac{1}{\dot{\tau}} \frac{R^2 + 16(1+R)/15}{(1+R)^2} \quad (11)$$

by which acoustic oscillations are damped exponentially as $\exp[-(k/k_D)^2]$. Notice that the diffusion length is roughly the geometric mean of the mean free path $\dot{\tau}^{-1}$ and horizon length η as one would expect of a random walk $k_D \sim \sqrt{\dot{\tau}/\eta}$.

2.2.2. Diffusion Damping during Recombination

As the universe recombines, the mean free path and hence the diffusion length of the photons increases. As long as the diffusion length is much greater than the mean free path, damping can be described by the tight-coupling approximation of the previous section. This is because the mean free path only surpasses the wavelength *after* diffusion has already destroyed the perturbations, resulting in no contributions outside of the tight-coupling regime. The approximation thus remains approximately true until quite near the end of recombination when the mean free path becomes comparable to the horizon and so the diffusion length (HSa, HSc). This fact explains the reasonable level of agreement between the numerical results we present in §2.3 and the tight-coupling approximation.

The remaining subtlety is that due to the finite duration of recombination, last scattering takes place at a slightly different epoch, with a slightly different diffusion length, for each photon. The net effect has been approximated (HSa) by weighting the damping by the visibility function $\dot{\tau}e^{-\tau}$, the probability of last scattering within $d\eta$ of η ,

$$\mathcal{D}(k) = \int_0^{\eta_0} d\eta (\dot{\tau}e^{-\tau}) \exp\{-[k/k_D(\eta)]^2\}. \quad (12)$$

This “smearing” of the last scattering surface, and the evolution of k_D tend to soften the damping, meaning it is not quite the simple exponential one would naively predict. It is however often convenient to define the last scattering epoch as $\tau(\eta_*) = 1$.

Notice that the net result depends only on the cosmological parameters of the background. The effect of $\Omega_0 h^2$ is simple. Increasing $\Omega_0 h^2$ decreases the horizon at last scattering thus monotonically decreasing the diffusion length. The dependence on $\Omega_b h^2$ is more complicated. Increasing $\Omega_b h^2$

1. decreases the mean free path
2. delays recombination
3. shortens its duration
4. speeds diffusion scale growth at recombination

The first effect tends to decrease the damping length and dominates for low $\Omega_b h^2$. The second effect extends the amount of time the photons can diffuse and hence increases the damping length; it dominates at high $\Omega_b h^2$. In the limit of instantaneous recombination, the damping function $\mathcal{D}(k)$ attains its sharpest form of $\exp\{-[k/k_D(\eta_*)]^2\}$. For the realistic case where recombination takes place over an extended period $\mathcal{D}(k)$ becomes less steep. Both the width of the visibility function and the evolution of k_D through it affect this drop. Again the baryon dependence of these two effects are in opposition leading to a steepening of the slope at both the high and low $\Omega_b h^2$ limits.

2.2.3. Free Streaming

After recombination photons enter the free-streaming regime. The observer views a temperature fluctuation at wavenumber k on the last scattering surface as an anisotropy at multipole moment $\ell \approx fkr_\theta(\eta_*)$, where the constant of proportionality $f \approx 0.98$ from numerical fitting (see §2.3) and the comoving angular-size distance to the epoch η is

$$r_\theta(\eta) = |K|^{-1/2} \sinh[|K|^{1/2}(\eta_0 - \eta)], \quad (13)$$

for $K < 0$. For positively curved universes, replace \sinh with \sin . The fact that angular size depends sensitively on the curvature allows its precise measurement from acoustic features (Doroshkevich, Zel’dovich & Sunyaev 1978, Sugiyama & Gouda 1992, Kamionkowski, Spergel & Sugiyama 1994, Hu & White 1996b). These effects are represented formally in the Boltzmann equation (1) by the transfer of power down the ℓ -hierarchy with distance $\eta - \eta_*$ from the last scattering event and the geodesic deviation factors κ_ℓ . Note that the latter becomes important when the distance is long enough such that the subtended angle $\theta \sim \ell^{-1} = \sqrt{K}/k$, i.e. smaller than that of a wavelength at the curvature distance.

The angular-size distance relation may be used to map k -space inhomogeneities onto ℓ -space anisotropies. For example, the damping function in multipole space is

$$\mathcal{D}_\ell \approx \mathcal{D}(k = \ell / fr_\theta(\eta_*)). \quad (14)$$

There are instances when this mapping fails to accurately describe the streaming process. The projection of k -mode inhomogeneities onto ℓ -mode anisotropies depends on the viewing angle and is thus not one-to-one. In particular, it can take power to larger angles for wavelengths that happen to be viewed with wavevector parallel to the line of sight. In this case, the angular separation between the intersections of the flat wavefront with the spherical shell at η_* is much larger than $(kr_\theta)^{-1}$. Sharp features in k -space will thus be blurred in ℓ -space and excess power at small physical scales can be aliased into large angular scales. Formally, this is reflected by the decomposition of the k -mode on the sphere and the fact that the solution to the sourceless Boltzmann or Liouville equation is just its radial component, a spherical Bessel function in flat space (see e.g. Bond & Efstathiou 1987). For the cases we consider, where the k -space features are broad with no strong deviations from scale invariance, the simple approximation of Eq. (13) suffices.

2.2.4. Reionization Damping

From the null detection of the Gunn-Peterson effect (Gunn & Peterson 1965), we know that the universe was reionized at least as early as redshift $z \approx 5$. Reionization recouples the photons to the electron-baryon plasma. The same process that is responsible for diffusion damping acts to destroy anisotropies during this epoch as well.

During the free-streaming epoch, the effective “diffusion length” is simply the horizon scale. Photon trajectories from different temperature regions on the last scattering surface intersect forming the anisotropy that is represented by the $\ell \geq 2$ photon modes. When the universe reionizes, the photons which rescatter lose their anisotropy. Note that the isotropic temperature fluctuation that exists above the horizon, where trajectories have not yet crossed, does not damp by rescattering. This is reflected in the lack of a $\dot{\tau}$ coupling term in the $\ell = 0$ mode of the Boltzmann equation (1). The $\ell = 1$ mode damps in such a way as to drive Θ_1 toward v_b so that the distribution is isotropic in the electron rest frame.

Even in a reionized universe, photons eventually last scatter as the electron density drops due to the expansion and the mean free path to scattering exceeds the horizon length. Thus only the fraction $e^{-\tau}$ of the photons that did not rescatter contribute to the anisotropy below the horizon at last scattering η_r . Above this scale all photons contribute. Thus the rough form of the reionization damping function becomes

$$\mathcal{R}_\ell = \begin{cases} 1 & \ell \ll r_\theta/\eta_r, \\ e^{-\tau} & \ell \gg r_\theta/\eta_r, \end{cases} \quad (15)$$

where again the effect of the finite duration of last scattering on η_r can be accounted for by the visibility function (see §2.4).

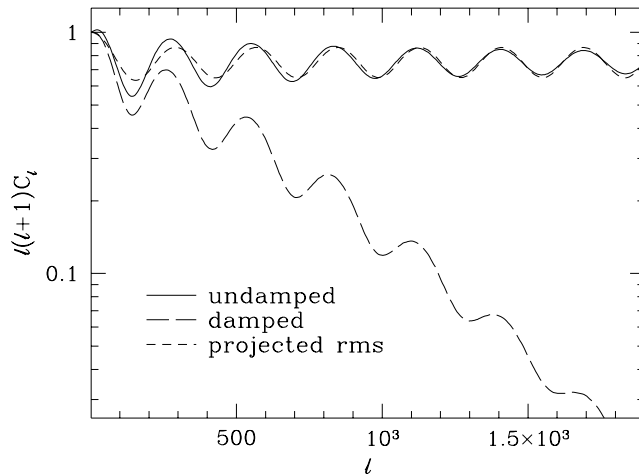


Fig. 1.— Diffusion damping calibration. In the absence of both diffusion damping and gravitational sources, the rms temperature fluctuation at recombination (short-dashed line) exhibits simple acoustic oscillations. These are mapped onto anisotropies on the sky in a near one to one fashion (solid line). The inclusion of diffusion terms in the Boltzmann equation allows for a simple numerical calibration of its effects.

2.3. Numerical Calibration

The expressions of the previous section are only approximations, though useful ones. We now turn to numerical calibration by solving the Boltzmann equations of §2.1.

Extracting the damping effects from realistic models of structure formation is complicated due to the manner in which gravity generates perturbations through the metric fluctuations Φ and Ψ in the model. Since the effects discussed above are essentially model-independent, we choose instead to calculate a toy-model in which no gravitational effects, beyond the background expansion, are included. Specifically, we solve the Boltzmann equations for the photons and baryons with $\Phi = 0 = \Psi$. This includes neglecting the self-gravity of the photon-baryon fluid.

Before recombination, we are left with a pure acoustic oscillation whose behavior is completely determined by the initial conditions. For simplicity, we take them to be adiabatic and scale invariant. The evolution equations of §2.1 are then solved in the usual way (see e.g. Bond & Efstathiou 1984, Ma & Bertschinger 1995, Seljak & Zaldarriaga 1996) through recombination to the present. This properly includes the effects of diffusion through the last scattering surface and the projection of the fluctuations at last scattering onto the sky today. We show an example in Fig. 1 (long-dashed line).

To extract the diffusion damping behavior, we compare this to a calculation of the same model with diffusion damping “turned off”. Specifically, we solve the tightly-coupled photon-baryon equation (5) up to the point where the optical depth to the present, (ignoring reionization) becomes unity. We then free-stream the photons to the present by solution of the sourceless Boltzmann equation ($\Psi = \Phi = \dot{\tau} = 0$ in Eqs. 1 and 2) to determine the anisotropy (see Fig. 1, solid line). The ratio of the angular power spectrum of the damped to undamped calculation gives the form of the damping function \mathcal{D}_ℓ^2 (see also Fig. 7). This also serves to

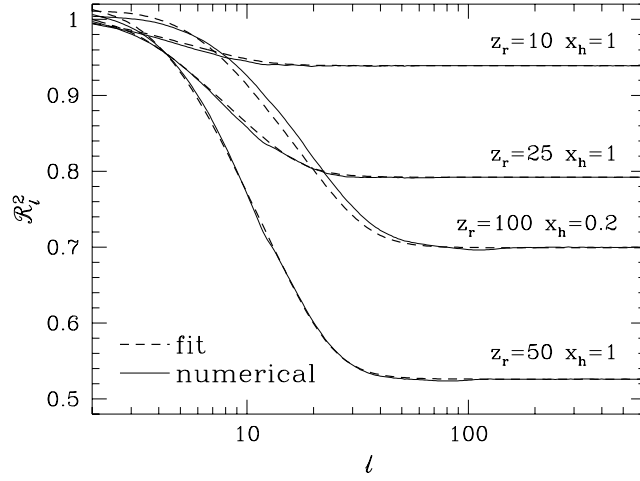


Fig. 2.— Reionization damping calibration. By removing the relative Doppler effect from a reionized Boltzmann calculation and comparing the result to the same model (here standard CDM $\Omega_0 = 1$, $h = 0.5$, $\Omega_b h^2 = 0.0125$) with no reionization, the effects of rescattering damping are isolated. The reionization damping envelope is fit by two parameters, the optical depth during reionization and the horizon scale at last scattering (see Eq. 24).

calibrate the angular-size distance relation of Eq. (13) through comparison with the mean squared fluctuations in Fourier space $|\Theta_0|^2 + |\Theta_1|^2/3$ at optical depth unity (see Fig. 1, short-dashed line). By aligning the peaks, one extracts the proportionality factor $f \approx 0.98$. As discussed in §2.2 free streaming smears features in the k -space rms spectrum somewhat which explains the slightly smoother actual anisotropy.

To extract the reionization damping behavior, we compare the no-reionization case to one with some arbitrary reionization history. In order to isolate damping effects from the Doppler effect due to the relative motion of the baryons with respect to the CMB, we set $v_b = \Theta_1$ during this epoch. For simplicity, we often parameterize the reionization as instantaneous at some epoch z_r to some constant fractional level of hydrogen reionization x_h though none of our results depend on this simplification. The ratio of the two power spectra gives \mathcal{R}_ℓ^2 . We show examples in Fig. 2 (solid lines).

2.4. Fitting Formulae

It is convenient to fit the numerical calculations of §2.3 for the diffusion damping and reionization damping envelopes. Aside from providing a compact summary of the results, this exposes the sensitivity of the spectrum to cosmological parameters which will be useful in §3.

2.4.1. Diffusion Damping Envelope

Since the effect of diffusion damping is determined solely through the Compton mean free path and horizon scale, it is dependent on very few cosmological parameters. The Compton mean free path of a photon is governed by the baryon density $\rho_b \propto \Omega_b h^2$. If the present energy density in the radiation is fixed, then the horizon only depends on the matter content $\Omega_0 h^2$ before curvature and cosmological constant contributions become significant. We assume here that the radiation energy density is fixed by the observed CMB temperature $T_\gamma = 2.728\text{K}$ (Fixsen et al. 1996) and there exist three families of massless neutrinos with $T_\nu = (4/11)^{1/3} T_\gamma$ (we ignore the small correction of Dodelson & Turner 1992). Thus aside from the projection effects from r_θ , which are sensitive to the curvature and cosmological constant, the damping behavior depends only on $\Omega_0 h^2$ and $\Omega_b h^2$. We have computed \mathcal{D}_ℓ as described in §2.3 for 150 models in the range $0.02 < \Omega_0 h^2 < 0.75$ and $0.005 < \Omega_b h^2 < 0.75$.

From the tight-coupling expansion, we expect the damping tail to scale as $\exp[-(\ell/\ell_D)^2]$. Including the effect of a finite last scattering surface and the conversion from k to ℓ makes the damping function less steep. We find that through the first two decades of damping in power, the function \mathcal{D}_ℓ calculated in the last section can be approximated as

$$\mathcal{D}_\ell = \exp[-(\ell/\ell_D)^m]. \quad (16)$$

The quantities $k_D f = \ell_D/r_\theta$ and m are functions of $\Omega_0 h^2$ and $\Omega_b h^2$ which are power laws at the extreme ends of parameter space (see Fig. 3). Recall that $f \approx 0.98$ is obtained by numerical calibration of the projection relation (see §2.3). We chose first to fit the $\Omega_b h^2$ dependence. A simple two-power law fit

$$\begin{aligned} \ell_D/r_\theta &= a_1(\Omega_b h^2)^{0.291}[1 + a_2(\Omega_b h^2)^{1.80}]^{-1/5}, \\ m &= a_3(\Omega_b h^2)^{a_4}[1 + (\Omega_b h^2)^{1.80}]^{1/5}, \end{aligned} \quad (17)$$

provides a good description of the numerically determined behavior. The coefficients of this fit are then functions of $\Omega_0 h^2$. We find that they fit single or double power-laws forms,

$$\begin{aligned} a_1 &= 0.0396(\Omega_0 h^2)^{-0.248}[1 + 13.6(\Omega_0 h^2)^{0.638}], \\ a_2 &= 1480(\Omega_0 h^2)^{-0.0606}[1 + 10.2(\Omega_0 h^2)^{0.553}]^{-1}, \\ a_3 &= 1.03(\Omega_0 h^2)^{0.0335}, \\ a_4 &= -0.0473(\Omega_0 h^2)^{-0.0639}. \end{aligned} \quad (18)$$

Together these fitting functions work to the percent level for $0.02 < \Omega_0 h^2 < 0.75$ and $0.005 < \Omega_b h^2 < 0.75$ and improve upon the approximate results of §2.2 and HSc (Eq. E4).

To complete the description of the damping, we need to express explicitly the conversion of physical to angular space variables through the angular-size distance r_θ . The missing ingredient of Eq. (13) is the comoving distance to the last scattering surface $\eta_0 - \eta_*$. The horizon scale today can be expressed as an integral over the Hubble parameter $\eta_0 = \int_0^1 (a^2 H)^{-1} da$. For $\Omega_\Lambda = 0$, this has the exact solutions

$$\eta_0 = \begin{cases} \frac{1}{H_0(1 - \Omega_0)^{1/2}} \ln \left[\frac{2 - \Omega_0 + 2(1 - \Omega_0)^{1/2}(1 + a_{\text{eq}}\Omega_0)}{\Omega_0 + 2(1 - \Omega_0)^{1/2}(a_{\text{eq}}\Omega_0)^{1/2}} \right] & K < 0, \\ \frac{1}{H_0(\Omega_0 - 1)^{1/2}} \left[\tan^{-1} \frac{\Omega_0^{1/2}(\Omega_0 - 1)^{-1/2}}{2a_{\text{eq}}^{1/2}(1 + a_{\text{eq}})^{1/2}} - \tan^{-1} \frac{2 + 2a_{\text{eq}} - \Omega_0 - 2a_{\text{eq}}\Omega_0}{2(1 + a_{\text{eq}})(\Omega_0 - 1)^{1/2}} \right] & K > 0, \end{cases} \quad (19)$$

while for $K = 0$, the following form,

$$\eta_0 = 2(\Omega_0 H_0^2)^{-1/2}[(1 + a_{\text{eq}})^{1/2} + a_{\text{eq}}^{1/2}](1 - 0.0841 \ln \Omega_0), \quad (20)$$

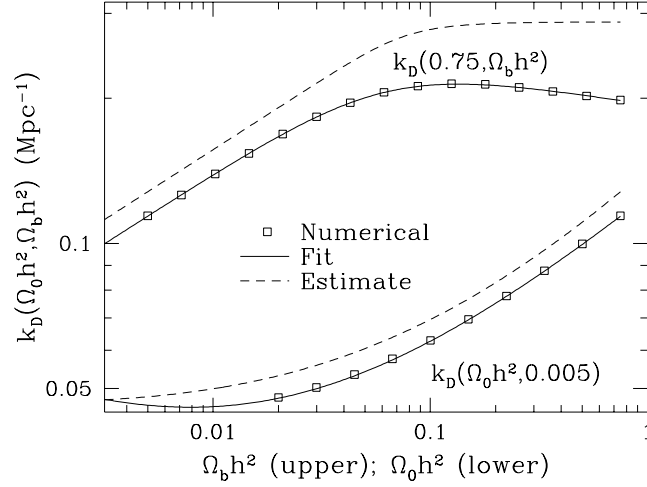


Fig. 3.— Diffusion scale calibration. Analytic estimates of $k_D(\Omega_0 h^2, \Omega_b h^2)$ based on the tight-coupling approximation trace the results to reasonable accuracy and explains their general behavior (HSc, Eq. E4). The fitting function of Eq. (17) tracks the numerical calibration to better than the 1% level.

fits the integral over the region $0.1 \lesssim \Omega_0 \leq 1$ and $0.3 \lesssim h$ to better than 1% accuracy. Here

$$a_{\text{eq}} = 4.17 \times 10^{-5} (\Omega_0 h^2)^{-1} (T_\gamma / 2.728 \text{K})^4 \quad (21)$$

is the scale factor at matter-radiation equality. Finally, the horizon at last scattering where $\tau(\eta_*) = 1$ takes the form

$$\eta_* = 2(\Omega_0 H_0^2)^{-1/2} [(a_* + a_{\text{eq}})^{1/2} - a_{\text{eq}}], \quad (22)$$

where (HSc, Eq. E1)

$$\begin{aligned} z_* &\equiv a_*^{-1} - 1 = 1048[1 + 0.00124(\Omega_b h^2)^{-0.738}][1 + b_1(\Omega_0 h^2)^{b_2}], \\ b_1 &= 0.0783(\Omega_b h^2)^{-0.238}[1 + 39.5(\Omega_b h^2)^{0.763}]^{-1}, \\ b_2 &= 0.560[1 + 21.1(\Omega_b h^2)^{1.81}]^{-1}, \end{aligned} \quad (23)$$

is a fit to the redshift of recombination.

2.4.2. Reionization Damping Envelope

Reionization damping depends on two parameters, the total optical depth τ and the angular scale subtended by the horizon at last scattering during the reionization epoch $\theta_r \sim \ell_r^{-1}$. The asymptotic values given in Eq. (15) are highly accurate and thus we need only search for an interpolating function around ℓ_r . The following form fits the behavior in \mathcal{R}_ℓ^2 to better than 1% for late reionization

$$\mathcal{R}_\ell^2 = \frac{1 - e^{-2\tau}}{1 + c_1 x + c_2 x^2 + c_3 x^3 + c_4 x^4} + e^{-2\tau}, \quad (24)$$

with $x = \ell/(\ell_r + 1)$ and $c_1 = -0.276$, $c_2 = 0.581$, $c_3 = -0.172$, $c_4 = 0.0312$. Even the more extreme case of early reionization to a low ionization level is described well at the couple of percent level (see Fig. 2). High precision in the large optical depth limit is unnecessary since secondary anisotropies dominate in this limit.

The parameter $\ell_r = r_\theta(\eta_r)/\eta_r$ involves the visibility-weighted horizon at reionization

$$\eta_r = \frac{\int d\eta \eta (\dot{\tau} e^{-\tau})}{\int d\eta (\dot{\tau} e^{-\tau})}, \quad (25)$$

where the optical depth functions can be obtained by noting that

$$\dot{\tau} \equiv n_e \sigma_T a = 2.304 \times 10^{-5} \text{Mpc}^{-1} (1 - Y_p) \Omega_b h^2 (1 + z)^2 x_h. \quad (26)$$

Here $Y_p \approx 0.23$ is the primordial helium mass fraction and recall that x_h is the hydrogen ionization fraction and we assume that helium is not ionized. It is useful to note that for low redshifts $z_r \ll 100$ and constant ionization fraction, the optical depth may be integrated analytically to give

$$\tau = 4.61 \times 10^{-2} (1 - Y_p) x_h \frac{\Omega_b h}{\Omega_0^2} \left\{ 2 - 3\Omega_0 + (1 + \Omega_0 z_r)^{1/2} (\Omega_0 z_r + 3\Omega_0 - 2) \right\} \quad (27)$$

when $\Lambda = 0$ and

$$\tau = 4.61 \times 10^{-2} (1 - Y_p) x_h \frac{\Omega_b h}{\Omega_0} \left\{ [1 - \Omega_0 + \Omega_0 (1 + z_r)^3]^{1/2} - 1 \right\} \quad (28)$$

when $K = 0$. For higher redshifts, the contribution of the radiation to the expansion rate can make a few percent or greater correction.

3. Cosmological Information

Armed with the calibration of the effects of diffusion and reionization damping, we can now examine the information, both on cosmological parameters and models for structure formation, embedded in the small-scale anisotropy spectrum. We begin with a discussion of the assumptions that render diffusion and reionization damping model-independent for most models of structure formation (§3.1). By removing the effects of damping in such models, one uncovers striking signatures that contain essential information on the nature of fluctuations in the early universe (see also Hu & White 1996b). For illustrative purposes, we often employ variants of the standard CDM model, scale invariant initial adiabatic fluctuations $k^3 |\Psi(0, k)|^2 = \text{const.}$ in an $\Omega_0 = 1$, $h = 0.5$, $\Omega_b h^2 = 0.0125$ universe.

Baryon drag, which enhances alternate acoustic peaks (§3.2), can help separate adiabatic from isocurvature fluctuations, an important step in distinguishing inflationary models from cosmological defect models (see Hu & White 1996b, Hu, Spergel, & White 1996). It also probes the gravitational potential at last scattering. The underlying amplitude of the oscillations extracts information on the evolution of the gravitational potentials at horizon crossing through the potential envelope (§3.3).

The diffusion damping and reionization damping envelopes are themselves interesting because they provide essentially model-independent information about cosmological parameters, mainly the curvature of the universe (§3.4) and the epoch and extent of reionization (§3.5). In this section, we systematically treat these applications of the results from the damping calibration in §2.

3.1. Model Assumptions

We begin by examining the conditions under which the diffusion damping and reionization damping envelopes are model-independent to expose general guidelines for their use.

Only acoustic *oscillations* are damped by diffusion. This leaves untouched e.g. offsets in the zero point of the oscillations or anisotropies generated between the last scattering surface and the observer. In the former case, the $-\Psi$ offset provided by the potential is not damped because it represents gravitational redshifts which are picked up by the photons even as they diffuse in and out of potential wells. The baryons provide an inertia to the photon-baryon fluid which further offsets the oscillation. The Compton drag of the baryons on the photons increases the photon temperature inside gravitational potential wells by $-R\Psi$ leading to a zero-point shift that is not damped by diffusion for similar reasons. Together the redshift and drag effects explain why in the estimates of §2.2, it is $\Theta_0 + (1 + R)\Psi$ which suffers damping and not Θ_0 .

The time evolution of the potentials causes a shift of order $\ddot{\Psi}/k^2$ [see Hu & White 1996b, Eq. (25)]. If $R \gg |\ddot{\Psi}/k^2\Psi|$, it is negligible in comparison to baryon drag. Generally Ψ varies on the order of an expansion time such that $|\ddot{\Psi}/k^2\Psi| = \mathcal{O}[(k\eta)^{-2}] \ll 1$ for scales well inside the horizon at last scattering: $k\eta \gg 1$. Mixed terms of the order $R\dot{\Psi}/k$ also exist but are again generally smaller than the $R\Psi$ term. Since the intrinsic acoustic amplitude is of order the gravitational potential at sound horizon crossing $\Psi(k, r_s^{-1})$, the diffusion damping signature dominates over the undamped term if

$$\left| \frac{\Psi(k_D, r_s^{-1})}{\Psi(k_D, \eta_*)} \right| \gtrsim R \quad (29)$$

and

$$k^2 \left| \frac{\Psi(k_D, r_s^{-1})}{\ddot{\Psi}(k_D, \eta_*)} \right| \gtrsim 1, \quad (30)$$

which are generally satisfied by models whose potentials do not grow significantly well within the sound horizon. Notice that no assumption of coherence in the oscillation is necessary (Magueijo et al. 1996).

In principle, there is also a model-dependent effect since in the discussion above we have implicitly assumed a two-step process: first the acoustic oscillations are formed and then they are damped. This is generally called in the literature a “passive” approximation (Albrecht et al. 1995). If the model possesses a strongly time-varying potential inside the horizon, the underlying acoustic oscillations could still be forming as the diffusion length overtakes the wavelength. Usually this is a small effect, since most of the damping occurs at the instant of recombination so that the fluctuations generated during this short time are small.

Finally anisotropies generated between recombination and the present could be larger than the intrinsic acoustic signal, especially in the damping tail. This could occur due to the linear (Kaiser 1984) and non-linear (Sunyaev & Zel’dovich 1970, Vishniac 1987) Doppler effects in a reionized universe or time variations in the potential along the line of sight (Sachs & Wolfe 1967, Rees & Sciama 1968, Kaiser & Stebbins 1984). In models such as cold dark matter (CDM) with a near scale-invariant spectrum of adiabatic initial fluctuations, this is not a worry. The lack of excessive small scale power in the model makes early reionization and/or small-scale non-linearities that are responsible for such effects unlikely (Ceballos & Barcons 1994, Seljak 1996, Hu & White 1996a).

These types of considerations also apply to the reionization damping function \mathcal{R}_ℓ calculated in §2.3. By construction, this function isolates the rescattering damping effect during reionization and ignores any secondary effects that may regenerate fluctuations. Again, the Doppler effect due to the relative velocity of

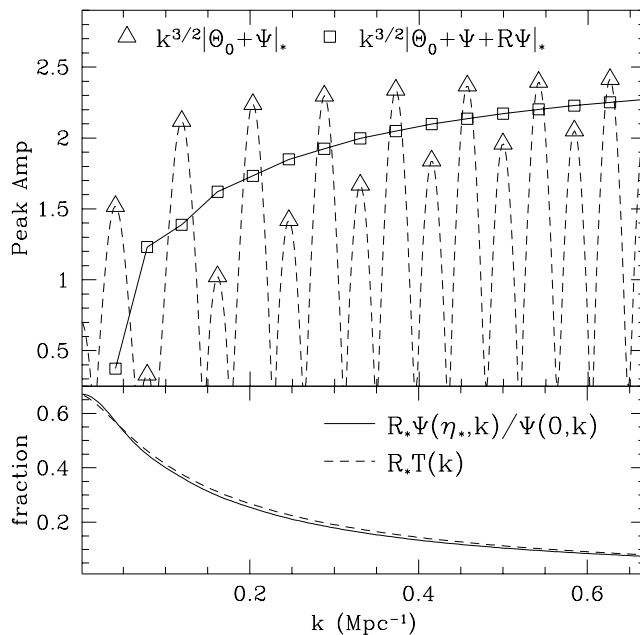


Fig. 4.— Baryon drag and its potential dependence. Baryon inertia in the fluid displaces the zero point of the temperature oscillations leading to alternating peak heights as a function of scale at last scattering. The magnitude of the displacement is $R_*\Psi(\eta_*)$, and by removing it the monotonic variation of heights due to the potential envelope is uncovered (upper panel). The fractional effect is of order $R_*\Psi(\eta_*, k)/\Psi(0, k)$ and can be adequately described by the matter transfer function $T(k)$ (lower panel). The model here is CDM with $\Omega_0 = 1$, $h = 1$ and $\Omega_b h^2 = 0.025$.

the electrons with respect to the CMB can regenerate fluctuations significantly if *both* the peculiar velocities and the optical depth are large. We examine this effect more closely in §3.5.

In summary, the damping function \mathcal{D}_ℓ accurately describes the model-independent damping of acoustic *oscillations* and the reionization damping function \mathcal{R}_ℓ does the same for the rescattering damping of *primary* anisotropies. In models such as CDM with no excess small scale power and hence relatively late reionization and small secondary effects, their behavior will be clearly manifest in the observable spectrum. In models where this is not true, it merely describes the behavior of a component of the total anisotropy and other effects must be taken into account to extract the information embedded in the observed anisotropy.

3.2. Uncovering the Baryon Signature

Baryons create a distinct acoustic signature due to the drag effect discussed in §3.1. By providing inertia to the fluid, they enhance compressions over rarefactions inside potential wells. Aside from providing a means to measure the baryon content, it also distinguishes between the two phases through the difference in peak amplitudes between successive peaks. In turn this distinction provides one of the most striking and

robust ways to distinguish adiabatic inflationary fluctuations from their isocurvature counterparts, generated perhaps by cosmological defects (Hu & White 1996b, Hu, Spergel, & White 1996). Unfortunately damping and projection effects serve to obscure this signal. By deconvolving these effects with the results and methods of §2.3-2.4, one can uncover this important signature.

Let us first examine the intrinsic effect. In Fig. 4, we show an example from a solution of the tight-coupling oscillator equation Eq. (5) under the metric fluctuations of an $\Omega_0 = 1$, $h = 1$, $\Omega_b h^2 = 0.025$ CDM model. Displayed is the effective temperature fluctuation of the peaks (triangles), connected by the full function to guide the eye. To demonstrate that the alternating height effect is due to baryon drag, we add $R_* \Psi(\eta_*, k)$ to each peak (squares), where $R_* = R(\eta_*)$. Notice that this eliminates the alternation, leaving the peak heights to smoothly vary in a manner described by the “potential envelope” discussed in the next section. Since the intrinsic amplitude of the oscillations is of order the potential before sound horizon crossing, the fractional effect is of order $R_* \Psi(\eta_*, k)/\Psi(0, k)$.

Since the effect depends on the potential at last scattering $\Psi(\eta_*, k)$, it also provides a probe of the matter fluctuations at that epoch. Under the CDM scenario, the potential does not evolve significantly between recombination and the present so that the baryon drag effect also reflects the matter fluctuations today. The fractional effect becomes $R_* \Psi(\eta_*, k)/\Psi(0, k) \approx R_* \Psi(\eta_0, k)/\Psi(0, k) = R_* T(k)$, where $T(k)$ is the matter transfer function (Bardeen et al. 1987),

$$T(q) = \frac{\ln(1 + 2.34q)}{2.34q} [1 + 3.89q + (16.1q)^2 + (5.46q)^3 + (6.71q)^4]^{-1/4}, \quad (31)$$

with $q = (k/\text{Mpc}^{-1})(T_\gamma/2.7\text{K})^2(\Omega_0 h^2)^{-1}$. In Fig. 4 (lower panel), we show that $RT(k)$ accurately tracks the effect and provides a potential consistency check with large scale structure today. As we shall see in the next section, the fall of the fractional baryon drag effect and the rise of the potential envelope are intimately related through the matter-radiation equality epoch.

The magnitude of the baryon drag effect in the observable anisotropy spectrum is reduced by inclusion of the dipole term and smoothing by projection, but mainly by diffusion damping. If the baryon content is low, the intrinsic magnitude of the effect is small and diffusion damping may cause the peak heights to monotonically decrease rather than alternate (see Fig. 5). Given the calibration of the diffusion damping behavior in §2.3, we can invert this filter. In Fig. 5, we show that multiplying the spectrum by \mathcal{D}_ℓ^{-2} uncovers the alternating peaks even for $\Omega_b h^2$ significantly lower than the standard big bang nucleosynthesis prediction. In practice, removing the damping behavior will require knowledge of $\Omega_0 h^2$ and $\Omega_b h^2$ either from external measurements or consistency checks (see Hu & White 1996b) as well as measurement of the curvature from the CMB.

3.3. Determining the Potential Envelope

Gravitational potential perturbations drive acoustic oscillations affecting their amplitude and phase. The effect on the phase can be used to uncover information about the origin of fluctuations in an inflationary epoch or phase transition (HSb, Crittenden & Turok 1995, Hu & White 1996b). Here we treat their effects on the *amplitude* of the intrinsic oscillations, unobscured by the presence of diffusion damping. This can be obtained from an observed spectrum by the techniques of §2 and is also useful for constraining the curvature (see §3.4)

As an example of the driving process, let us consider the case of adiabatic fluctuations. The self-

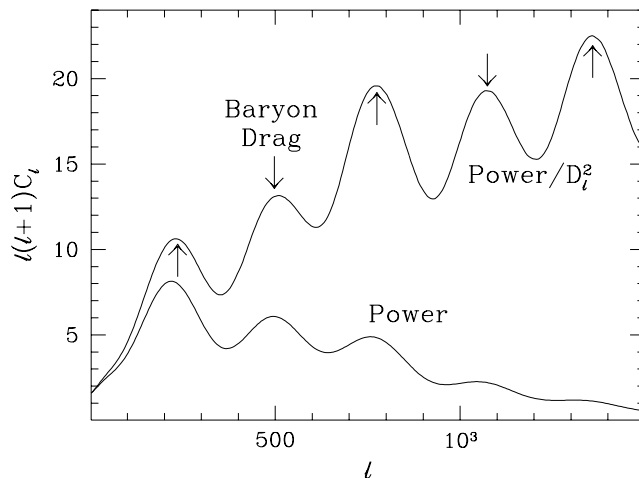


Fig. 5.— Uncovering Baryon Drag in a low baryon universe. Diffusion damping obscures the baryon drag signal especially in a low baryon universe (here $\Omega_b h^2 = 0.075$ in an otherwise standard CDM model). Employing the numerical calibration of the damping tail, we recover the alternations.

gravity of the photon-baryon fluid drives its own oscillations through a feedback mechanism at sound horizon crossing. Photon pressure prevents gravitational collapse inside the sound horizon leading to a decay in the self-generated gravitational potential. This decay is timed such that it leaves the oscillator in a highly compressed state leading to correspondingly large amplitude acoustic oscillations (see Hu & White 1996b for further description). If the self-gravity of the photons and baryons dominate, the amplitude of the oscillation is enhanced from gravitational redshifts by -2Ψ which combined with the Sachs-Wolfe effect (Sachs & Wolfe 1967) of $\frac{1}{3}\Psi$ yields a net result of $-\frac{5}{3}\Psi$, i.e. the amplitude of the oscillation should be 5 times the large-angle Sachs-Wolfe plateau. Inclusion of neutrinos and the matter-radiation transition modify this result to $5(1 + \frac{4}{15}f_\nu)^{-1}$, where the neutrino density fraction is $f_\nu = \rho_\nu/(\rho_\nu + \rho_\gamma)$ (HSc, Eq. B9). This driving effect only operates if the self-gravity of the photon-baryon fluid dominates at sound horizon crossing. Large scales cross the sound horizon in the matter-dominated epoch and do not suffer this effect. Thus the scale that crosses the horizon at matter-radiation equality k_{eq} marks the transition between the two asymptotic regimes.

The critical scale $k_{\text{eq}} = (2\Omega_0 H_0^2/a_{\text{eq}})^{1/2} \propto \Omega_0 h^2$ provides the CMB with sensitivity to the parameter $\Omega_0 h^2$. This is similar to the more familiar effect of equality on the matter power spectrum [see Eq. (31)] but note that fluctuations increase rather than decrease upon crossing k_{eq} . Fig. 6 shows that the potential envelope that governs the amplitude is indeed a function of $k/k_{\text{eq}} \propto k/\Omega_0 h^2$. Potentially, this effect can also probe the neutrino mass through its effect on k_{eq} (see Seljak & Bertschinger 1993, Ma & Bertschinger 1995, Dodelson, Gates & Stebbins 1995).

The remaining subtlety is that the presence of baryons makes acoustic oscillations decay adiabatically. Notice that the tight-coupling equation (5) describes an acoustic oscillator with effective mass of $(1+R)$. The adiabatic invariant for such an oscillator is the energy/frequency. This requires that temperature fluctuations decay as $(1+R)^{-1/4}$ and dipole or Doppler contributions to decay as $(1+R)^{-3/4}$. The amplitude of the

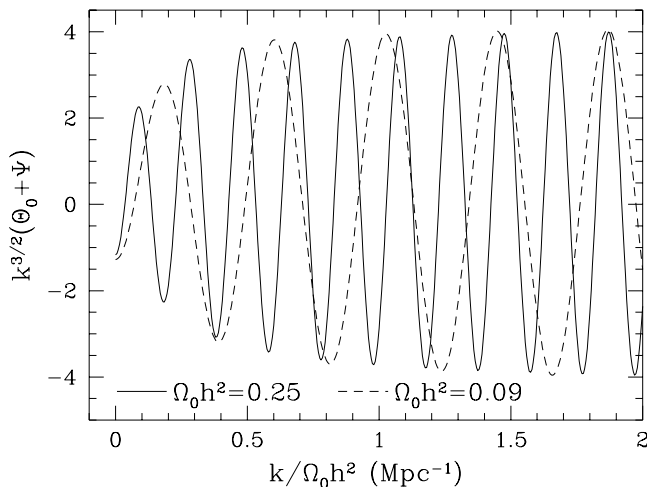


Fig. 6.— Potential Envelope. Decay of the potential due to the self gravity of the photon-baryon fluid drives the oscillator. Comparing two CDM models with differing matter to radiation ratios $\Omega_0 h^2$, we see that the oscillations are multiplied by an envelope that depends on the equality scale $k_{\text{eq}} \propto \Omega_0 h^2$.

potential envelope thus gains a baryon dependence set by the value of R at recombination (HSc).

The full potential envelope in power can be roughly described by

$$\mathcal{P}_\ell = 1 + A \exp(-1.4\ell_{\text{eq}}/\ell), \quad (32)$$

for a scale-invariant spectrum. Here $\ell_{\text{eq}} = k_{\text{eq}} r_\theta$ and the amplitude A is fixed by the asymptotic expression

$$A = 25(1 + \frac{4}{15}f_\nu)^{-2} \frac{(1 + R_*)^{-1/2} + (1 + R_*)^{-3/2}}{2} - 1, \quad (33)$$

where we have combined the temperature and Doppler effects in quadrature. Tilting the primordial spectrum produces an analogous tilt in \mathcal{P}_ℓ . The integrated Sachs-Wolfe effect (Sachs & Wolfe 1967) in open and Λ models, also gives \mathcal{P}_ℓ large-angle contributions (see also Hu, Sugiyama & Silk 1996).

We show an example in Fig. 7. The upper curves show a calculation with the effects of diffusion damping removed compared with the potential envelope of Eq. (33). Note that the form of the envelope roughly traces power in the fluctuations. The bottom curves show how diffusion damping obscures the signature and tests the damping calibration of §2.3 in a realistic context. By multiplying the undamped calculation by \mathcal{D}_ℓ^2 one regains, to reasonable accuracy, the result of a full CDM calculation incorporating diffusion damping.

Thus the obscuring effects of diffusion damping can be removed to extract the potential envelope of acoustic oscillations. This provides information on the evolution of the metric fluctuations as they cross the sound horizon which may help unravel information about the nature of such fluctuations in the general case and the scale of matter-radiation equality in the adiabatic case.

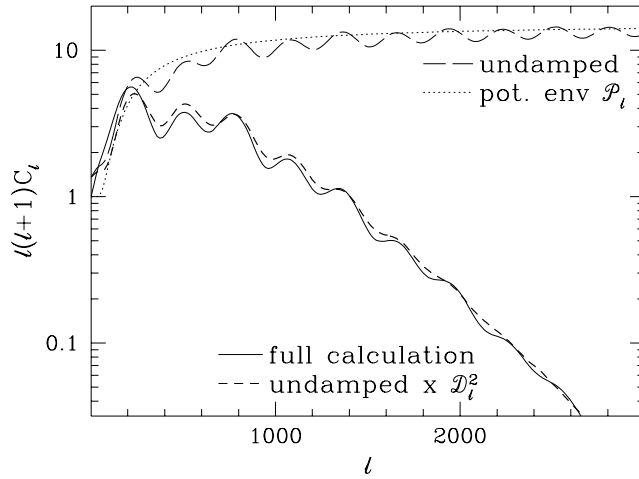


Fig. 7.— Uncovering the Potential Envelope. The potential envelope is obscured by diffusion damping. By numerically removing the damping, one sees that the intrinsic fluctuations follow the analytic estimates of \mathcal{P}_ℓ reasonably well. By multiplying by the numerically-calibrated damping function \mathcal{D}_ℓ^2 , one recovers the form of the full calculation even at very small angles. The model here is standard CDM.

3.4. Constraining the Curvature

The angular scale of diffusion damping ℓ_D provides a clear feature by which a classical angular-size distance test of the curvature can be made by comparison with the corresponding physical scale k_D (Hu & White 1996a). In models with simple acoustic peak features which can also be used for this test, this provides a consistency check on the curvature, important if the baryon content or thermal history of the universe is unknown or anomalous (Hu & White 1996b). In models where the peak signature is more complicated or non-existent (Albrecht et al. 1995), it may serve as the primary means of measuring the curvature.

In principle, the curvature is constrained by the simple absence or presence of small scale power. In an open universe, geodesic deviation moves the diffusion tail in angular space to smaller angles leading to more power on small scales. In practice, its application is complicated by secondary effects in the foreground and lack of *a priori* knowledge about the intrinsic amplitude of fluctuations before damping. The former is unlikely to be an obstacle in models with no strong non-linearities at small scales, in which the acoustic signal from recombination is the dominant contribution to the anisotropy.

Lack of knowledge of the intrinsic amplitude of oscillations limits the precision by which the curvature can be measured from the damping tail. The intrinsic amplitude is given by the potential envelope \mathcal{P}_ℓ discussed in the last section. Given that diffusion damping is exponential in ℓ , it takes only a rough estimate of \mathcal{P}_ℓ to yield interesting constraints on the curvature. Furthermore if \mathcal{P}_ℓ is a slowly varying function compared with \mathcal{D}_ℓ , measurement of the power on several scales in the damping tail can remove the ambiguity.

We show an example in Fig. 8. Here we assume that the underlying spectrum is of standard CDM which

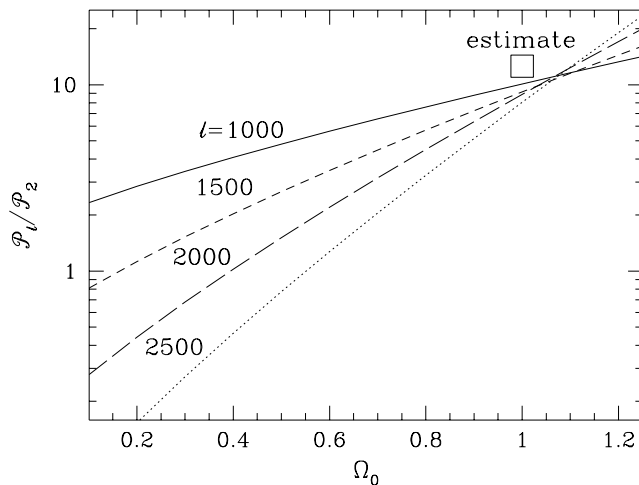


Fig. 8.— Constraining Ω_0 with the damping tail. By measuring the anisotropy power in at some scale ℓ in the damping tail (here averaged over 10% in ℓ) and comparing it to a reference scale (here $\ell = 2$), one determines the ratio of intrinsic powers $\mathcal{P}_\ell/\mathcal{P}_2$ before damping necessary to reproduce the observation (here $\Omega_0 = 1$ in standard CDM). Since this is a strong function of the assumed Ω_0 , only order of magnitude knowledge of the model-dependent intrinsic power is needed (e.g. square, estimated from Eq. (32)) to reject values of Ω_0 . Multiple measurements in the damping tail largely removes this ambiguity (curve intersection). For simplicity, we have fixed $h = 0.5$, $\Omega_b h^2 = 0.0125$ and $\Omega_\Lambda = 0$.

sets $\Omega_0 = 1$. By comparing the power at some scale ℓ in the damping tail to some reference scale, here $\ell = 2$,

$$\frac{\ell(\ell+1)C_\ell}{6C_2} = \frac{\mathcal{D}_\ell^2 \mathcal{P}_\ell}{\mathcal{D}_2^2 \mathcal{P}_2}, \quad (34)$$

and by using the fitting formula for \mathcal{D}_ℓ of Eq. (17), one can determine the intrinsic ratio of power $\mathcal{P}_\ell/\mathcal{P}_2$ as a function of Ω_0 needed to reproduce the measurement. We have ignored here the suppression of power from \mathcal{R}_ℓ as it is generally negligible for our purposes here. Because the damping multipole ℓ_D is a strong function of Ω_0 , the amount of intrinsic power required increases steeply with Ω_0 . Thus even the crude estimate of the CDM potential envelope of Eq. (32) is more than sufficient to distinguish between interesting values of Ω_0 (see Fig. 8, square). As the slope of the curves reflect, the further into the damping tail one can measure, the more powerful the test becomes. Of course for $\ell \gg \ell_D$, the signal also drops exponentially and hence is difficult both to measure and separate from secondary effects.

By measuring more than one scale in the damping tail, one obtains a consistency check on the curvature constraint. If the ℓ dependence of \mathcal{P}_ℓ is weak, as is the case for CDM-like scenarios (see Fig. 7), then the predictions for the intrinsic power must intersect near the actual value of Ω_0 . This implements the damping-tail shape test proposed in Hu & White 1996b to remove the model dependence of the curvature constraint. Even if only upper limits exist from CMB measurements at small scales, lower limits on Ω_0 can be obtained with reasonable assumptions on the amount of intrinsic power in small scale fluctuations.

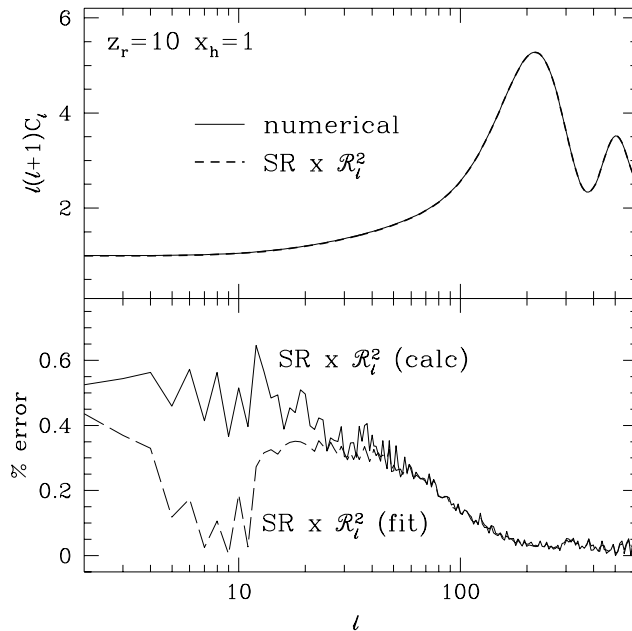


Fig. 9.— Reionization damping in standard CDM. Damping described by the envelope \mathcal{R}_ℓ is the main effect of late reionization in CDM type models. Hence employing either the numerical calibration of \mathcal{R}_ℓ and the fit to it from Eq. (24) to filter the results of a standard recombination (SR, no reionization) calculation approximate the full calculation to better than 1% in power. The scatter at low ℓ is a numerical artifact from finite sampling of the C_ℓ integral in k -space (see Eq. (4)).

3.5. Examining Reionization

Even late reionization produces potentially observable consequences for precise measurements of the CMB. In a standard CDM model, the optical depth ranges from 1-3% between $5 < z_r < 10$ leading to a 2-6% effect in the anisotropy power spectrum. For these low optical depths, it is likely that the main effect of reionization is the rescattering damping calculated in §2.3. In this case, two cosmological quantities are potentially extractable from the spectrum, the total optical depth and the horizon size at last scattering during the reionized epoch. In practice, extracting accurate results will be hampered by cosmic variance at large angles and the close degeneracy between changes in the spectrum due to the normalization and late reionization at small angles.

In Fig. 9, we show how well the numerical calibration of §2.3 and the fitting formula of §2.4 Eq. (24) reproduce the full effect of late reionization. The accuracy achieved is always better than a percent in power and increases toward small scales where the reionization signal is the largest. With the high precision achievable by the next generation satellite experiments, it is conceivable that the CMB spectrum can probe even such relatively late reionization.

If reionization occurs earlier, such that the optical depth is higher and/or non-linear effects dominate, then its effect on the CMB can be even more significant. Fluctuations are not only erased but also

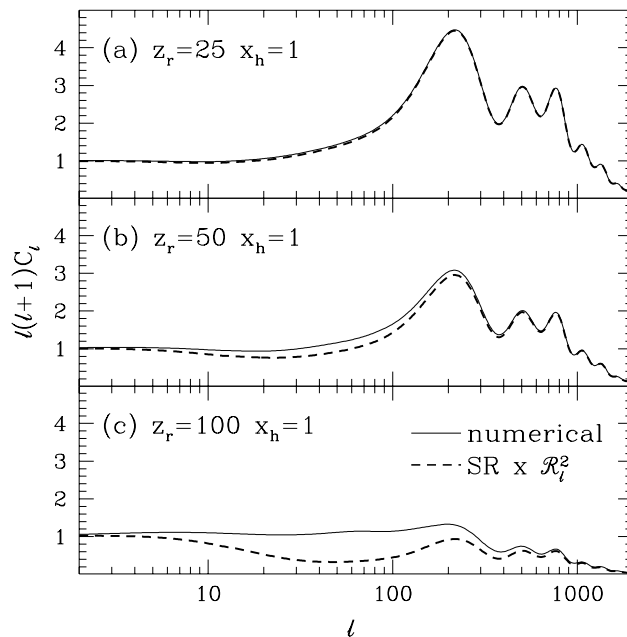


Fig. 10.— Reionization and the Doppler Effect. For early ionization, the Doppler effect due to the relative electron-photon velocity can regenerate fluctuations around the horizon scale at the last scattering epoch. By comparing the standard recombination (SR) result filtered by reionization damping \mathcal{R}_ℓ^2 to the full calculation, we can uncover such effects.

regenerated. As an example, consider the Doppler effect from the relative velocity of the electrons with respect to the CMB generated as the baryons fall into dark matter potential wells. Its effect peaks near the horizon at last scattering due to competing effects. Velocity flows are only generated inside the horizon. Yet on small scales, photons last scatter against many crests and troughs of the velocity perturbation leading to a strong cancellation damping of the Doppler effect (Kaiser 1984). By employing the rescattering damping function \mathcal{R}_ℓ from §2.3, we isolate this effect in Fig. 10. For the higher optical depth cases, the Doppler effect is clearly apparent as an excess of fluctuations from that predicted by \mathcal{R}_ℓ . On scales much smaller than the horizon at the last scattering epoch, simple analytic approximations exist for this effect (Kaiser 1984, Hu & White 1996a). In a CDM model where the optical depth is likely to be $\tau \lesssim 1$, such small scale effects are masked by larger primary anisotropies until well into the damping tail.

More complicated rescattering damping can occur if the reionization is patchy. Although one cannot directly apply the results of our damping calibration to this case, basic elements uncovered such as the dependence of damping on the horizon scale can be applied to this case as well. Non-linear effects can also create fluctuations through the Doppler effect but these are generally small in a model like CDM without excessive small scale power (but see Aghanim et al. 1996).

4. Conclusions

Prospects for measuring the small scale CMB anisotropy spectrum are bright, especially in light of the approval of two new satellite missions, MAP from NASA and Cobras/Samba from ESA, and the funding of ground based interferometers. If foregrounds, systematic and secondary effects are small or can be removed, and the inflationary CDM model is correct, much cosmological information can be extracted from the damping tail of CMB anisotropies (see e.g. Bersanelli et al. 1996). Despite the enormous success of this model however, it is quite possible that what is found there will come as a surprise to the current orthodoxy in cosmological modeling. In preparation for this possibility we have here, and in Hu & White 1996b, attempted to construct the spectrum out of fundamental physical effects that are likely to be the elements in any future model which successfully explains the observations.

The basic elements uncovered here represent a series of numerically calibrated transfer functions that describe the linear processing of fluctuations: the diffusion damping envelope, the reionization damping envelope, the potential envelope and the baryon drag modulation. The anisotropy spectrum is not merely a snapshot of conditions on the last scattering surface. Rather it is a dynamic entity that bears the mark of fluctuations before horizon crossing through the acoustic phase (Hu & White 1996b), at horizon crossing through the potential envelope, at last scattering through baryon drag, and after last scattering through the large-angle potential envelope (Sachs & Wolfe 1967) as well as the effects of reionization. Within the present framework of model possibilities, this view of its structure also creates a system of consistency checks by which we can verify model assumptions, such as the inflationary or cosmological defect origin of fluctuations, before proceeding to measure cosmological parameters and details of the model.

Acknowledgments: W.H. was supported by a grant from the W.M. Keck Foundation.

REFERENCES

- Aghanim, N., Desert, F. X., Puget, J. L. & Gispert, R. 1996, A&A, 311, 1 [astro-ph/9605083]
- Albrecht, A., Coulson, D., Ferreira, P., & Magueijo, J. 1996, Phys. Rev. Lett., 76, 1413 [astro-ph/9505030]
- Bardeen, J. M., Bond, J. R., Kaiser, N., & Szalay, A. S. 1987, ApJ, 304, 15
- Bersanelli, M. et al. 1996, ESA Phase A Study
(<http://astro.estec.esa.nl/SA-general/Projects/Cobras/report/report.html>)
- Bond, J. R. in Cosmology and Large Scale Structure, ed. by R. Shaeffer et al. (Elsevier Science Publishers, Netherlands) in press.
- Bond, J. R., & Efstathiou, G. 1984, ApJ, 285, L45
- Bond, J. R., & Efstathiou, G. 1987, MNRAS, 226, 665
- Bond, J. R., et al. 1994, Phys. Rev. Lett., 72, 13 [astro-ph/9309041]
- Ceballos, M. T., & Barcons, X. 1994, MNRAS, 271, 817
- Crittenden, R. G., & Turok, N. G. 1995, Phys. Rev. Lett., 75, 2642 [astro-ph/9505120]
- Dodelson, S., Gates, E., & Stebbins, A. 1996, ApJ, 467, 10 [astro-ph/9509147]
- Dodelson, S., & Turner, M. S. 1992, Phys. Rev., D46, 3372
- Doroshkevich, A. G., Zel'dovich, Ya. B., & Sunyaev, R. A. 1978, Sov. Astron., 22, 523
- Durrer, R., Gangui, A., & Sakellariadou, M. 1996, Phys. Rev. Lett., 76, 579 [astro-ph/9507035]
- Efstathiou, G., & Bond, J. R. 1987, MNRAS, 227, 33p
- Fixsen, D. J., et al. 1996, ApJ, [in press, astro-ph/9605054]
- Gunn, J. E., & Peterson, B. A. 1965, ApJ, 318, L11
- Hu, W., Scott, D., Sugiyama, N., & White, M. 1995, Phys. Rev. D., 52, 5498
- Hu, W., Spergel, D. N., & White, M. 1996, [astro-ph/9605193]
- Hu, W., & Sugiyama, N. 1995, ApJ, 444, 489 (HSa) [astro-ph/9406071]
- Hu, W., & Sugiyama, N. 1995, Phys. Rev. D, 51, 2599 (HSb) [astro-ph/9411008]
- Hu, W., & Sugiyama, N. 1996, ApJ(HSc) [in press, astro-ph/9510117]
- Hu, W., Sugiyama, N., & Silk, J. 1996, Nature, [in press, astro-ph/9604166]
- Hu, W., & White, M. 1996a, A&A, [in press, astro-ph/9507060]
- Hu, W., White, M. 1996b, ApJ[in press, astro-ph/9602019] Phys. Rev. Lett., 76, 1007 [astro-ph/9507080]
- Jungman, G., Kamionkowski, M., Kosowski, A. & Spergel, D. N. 1996, Phys. Rev. D., 54, 1332 [astro-ph/9512139]

- Kaiser, N. 1983, MNRAS, 202, 1169
- Kaiser, N. 1984, ApJ, 282, 374
- Kaiser, N. & Stebbins, A. 1984, Nature, 310, 391
- Kamionkowski, M., Spergel, D. N., Sugiyama, N. 1994, ApJ, 426, L57 [astro-ph/9401003]
- Ma, C. P. & Bertschinger, E. 1995, ApJ, 455, 7 [astro-ph/9506072]
- Magueijo, J., Albrecht, A., Coulson, D., & Ferreira, P. 1996, Phys. Rev. Lett., 76, 2617 [astro-ph/9511042]
- Peebles, P. J. E. & Yu, J. T. 1970, ApJ, 162, 815
- Rees, M. J. & Sciama, D. N. 1968, Nature, 217, 511
- Sachs, R. K. & Wolfe, A. M. 1967, ApJ, 147, 73
- Seljak, U. 1994, ApJ, 435, L87 [astro-ph/9406050]
- Seljak, U. 1996, ApJ, 460, 549 [astro-ph/9506048]
- Seljak, U., Bertschinger, E. 1993, Proceedings of “Present and Future of the Cosmic Microwave Background”, Santander, Spain, ed. J.L.Sanz, E.Martinez-Gonzalez, L.Cayon, (Springer Verlag, Berlin), p.165
- Seljak, U. & Zaldarriaga, M. 1996, astro-ph/9603033
- Silk, J. 1969, ApJ, 151, 459
- Sugiyama, N. & Gouda, N. 1992, Prog. Theor. Phys., 88, 803
- Sunyaev, R. A. & Zel’dovich 1970, Ya. B., Astrophys. Space Sci. 7 1
- Vishniac, E. T. 1987, ApJ, 322, 597
- Weinberg, S. 1972, Gravitation and Cosmology (Wiley, New York) p. 568
- White, M., & Scott, D. 1996, ApJ, 459, 415 [astro-ph/9508157]
- Wilson, M. L. 1983, ApJ, 273, 2

whu@sns.ias.edu

<http://www.sns.ias.edu/~whu>